https://doi.org/10.5194/egusphere-2024-3984
Preprint. Discussion started: 28 January 2025

Identifying controlling climate factors conducive to water and nitrogen export from agricultural watershed during snowmelt runoff period by using the SWAT model

Qiang Zhao[1,2], Dan Chang[1,3], Zhenyang Peng[1,3], Qian Yao [3], Jingwei Wu[1*], Chenyao Guo[1], Chengeng Li[1,4]

[1] School of Water Resources and Hydropower Engineering, Wuhan University, Wuhan, Hubei, 430072 China;
[2] Yangtze Eco-Environment Engineering Research Center, China Three Gorges Corporation; Wuhan, Hubei, 430010 China;
[3] Changjiang Institute of Survey, Planning, Design and Research, Wuhan, 430010 China
[4] Liaoning River and Reservoir Management Service Center, Liaoning Hydrological Bureau, Shenyang 110003, China

Correspondence to: Jingwei Wu (jingwei.wu@whu.edu.cn)

Abstract. Temperature and precipitation variations during the freezing-thawing period affect snowmelt and accompanying nitrogen export in a complex manner. These influences can be long-lasting, superimposed, and strengthened. Daily discharge and nitrate nitrogen NO_3^--N concentrations were monitored during the snowmelt periods of 2015 and 2016 in an agricultural watershed in northeastern China. The SWAT model was used to simulate the water and NO_3^--N export during the snowmelt period of 1951–2014 to identify the controlling climate factors and confirm their suitable combination that facilitates snowmelt water and NO_3^--N export. Our results show that the SWAT model performs well for *Re* values in simulating the daily snowmelt runoff and NO_3^--N export, but poorly for *NSE* and R^2 values in simulating NO_3^--N export. This is attributed to the absence of snowmelt water refrozen and hysteresis modules. The number of days and precipitation of the stable freezing period and the stating day of snowmelt period are controlling factors of daily snowmelt runoff, while daily NO_3^--N export are mostly affected by precipitation during the snowmelt period. The combinations of climatic factors favored by snowmelt runoff and NO_3^--N export were different. Years with longer stable freezing periods, later snowmelt period starting days, and higher rainfall during snowmelt, more readily generated high snowmelt runoff. Correspondingly, later appeared, higher and concentrated rainfall events, and higher temperatures between these rainfall and snowmelt events favored the NO_3^--N export. Finally, this study is of great importance for the prevention of spring floods and water pollution during snowmelt periods.

1. Introduction

Snowmelt water is a major water source for cold regions (Sterle et al., 2019; Heggli et al., 2022), and is used for domestic purposes (Cao et al., 2013), agricultural irrigation (Qin et al., 2020), recreation (Ligare et al., 2012), hydropower generation (Rheinheimer et al., 2014), and groundwater recharge (Lone et al., 2021). Snowmelt is consistently accompanied by remarkable nitrogen export in seasonally frozen agricultural watersheds (Zhao et al., 2017; Zhao et al., 2022), which may

https://doi.org/10.5194/egusphere-2024-3984
Preprint. Discussion started: 28 January 2025

result in significant nitrogen losses and adverse impacts on terrestrial and aquatic ecosystems (Corriveau et al., 2011; Rattan et al., 2017).

Water and nitrogen sources and migration paths during the snowmelt period are notably affected by variations in climatic factors. A 0.8–1.2 °C increase in global air temperature has occurred compared with the pre-industrial levels (IPCC, 2018), and the precipitation has been predicted to increase during winter over some cold regions of the Northern Hemisphere (Räisänen and Eklund, 2011; Rasouli et al., 2015). During the freezing period, higher temperatures decrease the proportion of snowfall to total precipitation (Irannezhad et al., 2017; Romshoo et al., 2022), increase the occurrence of rain-on-snowmelt events (Dou et al., 2021), and change the storage form of surface water (ice or snow) (Zhao et al., 2021). This results in reduced snow cover area, snow cover duration, snow water equivalent, and nitrogen wet-deposition, and may finally alter the available water and nitrogen sources to generate before snowmelt in space and time (Clement et al., 2012; Klein et al., 2016; Aygun et al., 2020; Zhao et al., 2021). Moreover, the depth of snow cover influences soil temperatures owing to its insulating property, while also influencing the freezing and thawing of soil (Li et al., 2022). This can alter the water and nitrogen storage in the surface soil since soil freezing can result in an upward movement of soil water (Bing et al., 2015; Ireson et al., 2013), reduced soil evaporation, and restrained infiltration capacity (Appels et al., 2018; Ploum et al., 2019; Zhang et al., 2019). During the thawing period, a warmer climate advances the occurrence time of snowmelt events (Uzun et al., 2021; Vorkauf et al., 2021; Yang et al., 2022). Temperature and precipitation variations can also affect the migration of water and nitrogen by altering the thawing depth of frozen soil, which markedly influences the infiltration, flow paths, and groundwater table variability (Koch et al., 2013; Koch et al., 2015; Wright et al., 2010).

The responses of snowmelt and the corresponding nitrogen export processes to temperature and precipitation variations during the freezing-thawing period are markedly different from those of rainfall runoff during warm periods (Chen et al., 2012; Zhao et al., 2021; He et al., 2022; Zhao et al., 2022). The influence of rainfall on water and nitrogen export lasts only for days or tens of days, and weakens over time (Chen et al., 2012; He et al., 2022). The influence of climate variation during the freezing-thawing period on snowmelt can last for several months, and the influences may even be strengthened during the freezing period. For example, Pittman et al. (2020) found that antecedent moisture affected by autumn rain controls infiltration and flow initiation, timing, and magnitude in frozen macroporous soils. Zhao et al. (2021) discovered that high autumn rainfall and temperature rise during the stable freezing period induced a long-term, gradually increasing, and higher runoff ratio of the ice melt runoff process during the thawing period. These studies mostly focused on the hydrological and nitrogen generation processes induced by single climate variation events (rain-on-snow, temperature rise, or autumn rain), or the prediction of their response to future climate change by numerical models (Li et al., 2016; Wang et al., 2018; Dou et al., 2020; Yang et al., 2022), but did not consider the interaction and superposition functions of changes in temperature and precipitation at different freeze-thaw periods on the sources and migration pathways of water and nitrogen during the snowmelt process. Further, it unclear whether there is a suitable combination of different climatic factors at different freezing-thawing periods that facilitates the production of water and nitrogen.

https://doi.org/10.5194/egusphere-2024-3984
Preprint. Discussion started: 28 January 2025

The lack of long-term monitoring data of daily water and nitrogen export during the snowmelt period in cold regions is the main reason for limiting research on the above questions. Therefore, using hydrological and water quality models, limited observed daily water and nitrogen generation data, and long-term climate data to expand the water and nitrogen export dataset is a compensatory solution to this dilemma (Shrestha et al., 2012; Dibike et al., 2021). Soil and Water Assessment Tool (SWAT) model is a physically-based hydrological model (Arnold et al., 2012). It contains a snowmelt and nitrogen migration and transformation module and is widely used in the modeling of snowmelt runoff and nitrogen export processes in cold regions (Bhatta et al., 2019; Shrestha and Wang, 2020; Zaremehrjardy et al., 2022). Ouyang et al. (2013) applied the SWAT model to quantify the non-point nitrogen variation induced by land-use change in a freeze-thaw area. Crusson et al. (2015) assessed the capability of the SWAT model to simulate snow cover and snowmelt dynamics over an alpine watershed, and found that SWAT produced a good spatial and temporal representation of the snow cover. Mukundan et al. (2020) used a modified version of the SWAT model to investigate the impact of climate change on nutrient loading in the Cannonsville Reservoir watershed of New York City. However, these studies mostly used the SWAT model to simulate the production of water and nitrogen annually and monthly; its suitability for the simulation of water, especially nitrogen export on a daily scale, needs to be further tested.

In this study, daily discharge and NO_3^--N concentration were monitored during the snowmelt period of 2015 and 2016 in the sub-basin of the Heidingzi watershed in northeastern China, and the SWAT model was used to simulate the water and nitrogen export during the snowmelt period of 1951–2014 to (1) evaluate the applicability of the SWAT model to simulate daily water and NO_3^--N export; (2) identify the controlling climate factors of snowmelt and NO_3^--N export and their influencing mechanism; and (3) confirm the suitable combination of different climate factors at different freezing-thawing periods that facilitate the production of water and NO_3^--N.

2 Material and methods

2.1 Study area and data collection

An agricultural watershed (6.84 km^2) located in Shuangyang District, Changchun, Jilin Province, China--within the latitude-longitude range of 125°34′27″–125°42′22″E, 43°22′48″–43°29′37″N--was selected for this study. The watershed elevation ranged from 234–380 m, with an average slope of 8.3°. The average annual temperature and precipitation (1951–2016) were 4.8 °C and 624.7 mm (~8% snow and 92% rain), respectively. The freezing-thawing period lasts from mid-November to early March, and the mean temperature and precipitation during this period were −10.5 °C and 31.8 mm, respectively. Maize fields, rural areas, and forests are the major land uses, accounting for 80.4%, 16.7%, and 2.9% of the total area. The soils in the watershed are mainly meadow, white mud, and dark brown soils (Fig. 1).

The basic datasets required to set the model input files were the topography, land use, soil, and climatic data. The digital elevation model (DEM) used in the study area was obtained from the International Scientific Data Service Platform (wist.echo.nasa.gov) with a resolution of 30 × 30 m. Land use data (30 × 30 m) were obtained from the Landsat thematic

https://doi.org/10.5194/egusphere-2024-3984
Preprint. Discussion started: 28 January 2025

mapper image data acquired in 2012. Soil data were obtained from the second soil survey conducted in Jilin Province. Daily climatic data (including precipitation, minimum and maximum temperatures, solar radiation, wind speed, and relative humidity) were obtained from the Shuangyang weather station which is 12 km away from the study area. The recording period was 1961–2016. Daily streamflow and NO_3^--N load datasets during the thawing period of 2014–2015 and 2015–2016 were obtained by flow discharge measurements and water sample collection and analysis at the watershed outlet. There was no point source pollution in the study watershed, and fertilizer and manure application rates were obtained through sampling surveys with farmers.

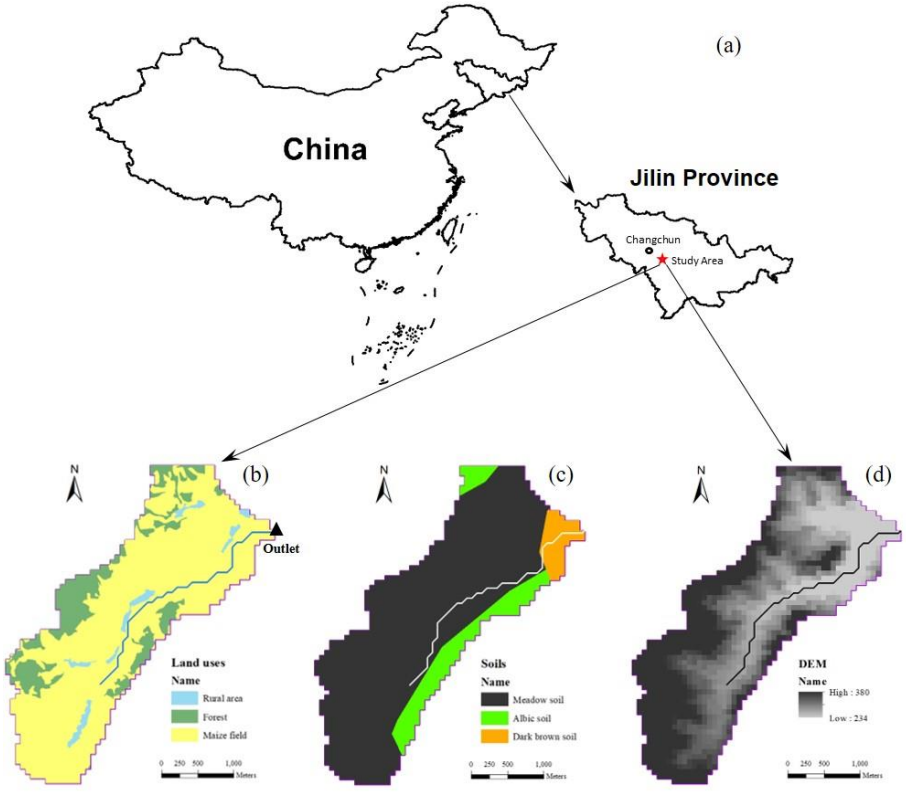

Fig. 1 Study site description. (a) Location of the watershed in China; (b) land uses, (c) soil, and (d) topography of the study watershed

2.2 General research framework

Figure 2 shows a technology route map of the study process. Meteorological data, observed daily water, NO_3^--N export data during the snowmelt period of 2014–2015 and 2015–2016, and GIS data were used to setup the SWAT model. Application of the SWAT model to simulate daily snowmelt runoff and NO_3^--N export was evaluated during the calibration and validation processes. Different freeze-thaw periods were divided using past climate data (1951–2014), corresponding climate

https://doi.org/10.5194/egusphere-2024-3984
Preprint. Discussion started: 28 January 2025

factors were calculated, and daily water and NO_3^--N export were simulated. On this basis, the controlling climate factors of snowmelt and NO_3^--N export were identified, and a suitable combination of different climate factors that facilitate the production of water and NO_3^--N was confirmed.

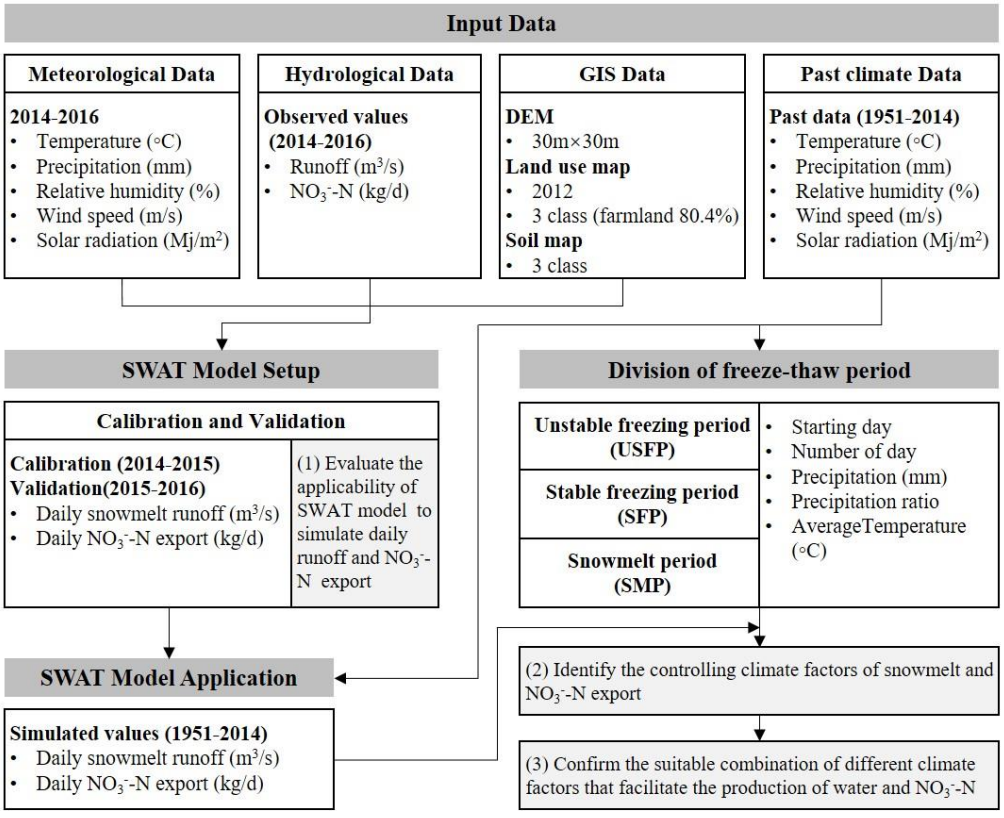

Fig. 2 Technology route map of the study process

2.3 SWAT setup

For modeling purposes, the SWAT model partitions a watershed into a number of sub-watersheds or sub-basins, which are further partitioned into a series of hydrologic response units (HRU) with unique land cover, soil, and agricultural management practice combinations. The generation of surface runoff, soil water, groundwater, sediment, and nutrients is calculated in every HRU and then routed through the river channel.

Data from a 30-m DEM obtained from geospatial data cloud of Chinese Academy of Sciences were used to delineate and discretize the study watershed into sub-watersheds using the ArcSWAT interface, and the land use, soil, and slope maps were imported and overlaid to derive different HRUs. Since this study only simulated the freezing-thawing period, i.e., the fallow period, it did not involve the planting, management, and harvesting of crops, and only one fertilization event occurred before spring plowing around April 8 yearly. The amount of nitrogen fertilizer applied was 60 kg/ha. The amount of manure

https://doi.org/10.5194/egusphere-2024-3984
Preprint. Discussion started: 28 January 2025

added was 0.277 kg/(ha.day), and of this total amount of manure, 39.4% was produced by beef cows, followed by mutton sheep (23.6%), human (18.4%), pigs (11.6%), and poultry (0.7%). Input climatic datasets of daily precipitation, temperature (minimum and maximum), solar radiation, wind speed, and relative humidity were used to run the model. Initial values of soil moisture, soil nutrient, and groundwater depth of each year were set to be consistent with the monitoring data in the autumn of 2015. Finally, the following modeling options were implemented during the model setup: surface runoff was calculated using the curve number model on a daily timescale. Potential evapotranspiration was estimated using the Hargreaves method, which uses only temperature data (Hargreaves et al., 1985).

2.4 SWAT calibration, and validation

2.4.1 Sensitivity analysis

Numerous parameters are used in the SWAT model. Sensitivity analysis was performed to identify the main influencing parameters. Potential impact parameters were obtained from papers focusing on hydrology and non-point nitrogen modeling using the SWAT model in cold regions. A sensitivity index was used to evaluate the sensitivity of the parameters.

$$S_{AF} = \frac{\Delta A / A}{\Delta F / F} \quad (1)$$

Here, S_{AF} represents the sensitivity index; F and ΔF represent the parameter and percentage adjustment of the parameter being considered, respectively; and A and ΔA represent the model output values predicted with F and $F + \Delta F$, respectively. The value of S_{AF} ranges from - ∞ to + ∞. A positive and negative sensitivity indicates that the parameter has the same and inverse effects on the prediction, respectively. Fifteen parameters that had the greatest impact on water discharge and NO_3^--N export are shown in Tables A1 and A2.

2.4.2 Statistical evaluation

The performances of the modeling of water discharge and NO_3^--N export were assessed according to three coefficients of accuracy: R^2, *NSE* and R_e as follows:

$$R^2 = \left(\frac{\sum_{i=1}^{n} \left(O_i - O_{avg}\right) \cdot \left(P_i - P_{avg}\right)}{\left[\sum_{i=1}^{n} \left(O_i - O_{avg}\right)^2 \cdot \sum_{i=1}^{n} \left(P_i - P_{avg}\right)^2 \right]^{0.5}} \right)^2 \quad (2)$$

Where O_i and P_i represent the observed and predicted values, and Q_{avg} and P_{avg} are the averages of the observed and predicted values, respectively. R^2 represents the proportion of total variance in the observed data, which can be explained by the model. It ranges between 0.0–1.0; higher values indicate better performance.

https://doi.org/10.5194/egusphere-2024-3984
Preprint. Discussion started: 28 January 2025

$$NSE = 1 - \frac{\sum_{i=1}^{n}\left(O_i - P_i\right)^2}{\sum_{i=1}^{n}\left(O_i - O_{avg}\right)^2} \quad (3)$$

NSE indicates how well the plot of observed values versus simulated values fits the 1:1 line (Nash and Sutcliffe, 1970). It ranges from -∞ –1, and larger values are indicative of better model performance.

$$Re = \frac{\left(P_{avg} - O_{avg}\right)}{O_{avg}} \cdot 100\% \quad (4)$$

Re is a measure of the accumulation of differences between the observed and simulated values for a particular period of analysis.

2.4.3 Calibration and validation

This study only simulated snowmelt runoff during the snowmelt period. Therefore, the observed datasets of water discharge and NO_3^--N export during the snowmelt periods of 2014–2015 and 2015–2016 were used for calibration and validation, respectively. Simulation results are considered to be good if *NSE* values are greater than 0.75, and satisfactory for *NSE* values between 0.75–0.36. For *Re* and R^2, values < ±20% and >0.5 are considered satisfactory (Levesque et al., 2008; Van Liew et al., 2003). For this study, $R^2 > 0.5$, *NSE* > 0.5, and *Re* < ±20% were considered acceptable for daily snowmelt runoff simulation, and $R^2 > 0.4$, *NSE* > 0.36, and *Re* < ± 20% were considered acceptable for daily NO_3^--N export simulation. The process of parameter calibration and validation is illustrated in Fig. 3.

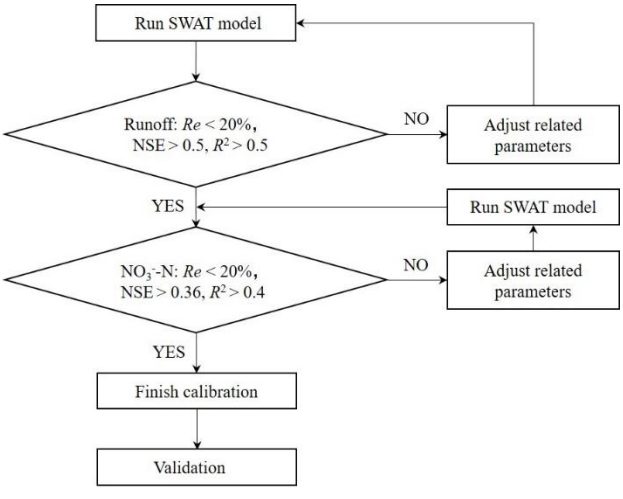

https://doi.org/10.5194/egusphere-2024-3984
Preprint. Discussion started: 28 January 2025

Fig. 3. Process of calibration and validation of daily snowmelt runoff and NO_3^--N export.

2.5 Statistical analyses

Coefficients of principal component regression between climate factors and runoff, runoff coefficient, and NO_3^--N export were calculated using SPSS17 to identify the major affecting factors. The Mann-Kendall (MK) test method was used to analyze the variation trend of climate factors, snowmelt runoff and NO_3^--N export. A detailed calculation process of MK test method has been reported by Shi et al. (2019).

3. Results

3.1 Snowmelt water and NO_3^--N export calibration

Tables 1 shows the optimum parameter values used in the daily snowmelt runoff and NO_3^--N export simulations. The observed and simulated daily runoff and NO_3^--N export for the calibration period (2014–2015) and validation period (2015–2016) are shown in Fig. 4. The statistical evaluation of the model performance based on the daily runoff and NO_3^--N export is presented in Table 2. Simulated daily runoff mostly displays consistent variations with observed values during the snowmelt period of both 2014–2015 and 2015–2016. However, snowmelt runoff is always overestimated during some initial snow-melting days when the temperature drops to subzero. Meanwhile, snowmelt runoff is underestimated during the flowing temperature rise days. The *NSE*, R^2, and R_e values were 0.75, 0.78, and -12.76% for the daily snowmelt runoff calibration and 0.54, 0.51, and 15.65% for validation, respectively. The performance of SWAT in modelling daily NO_3^--N export was not as good as that in modelling daily runoff. The *NSE*, R^2, and R_e values were -0.19, 0.44, and 2.7% for daily NO_3^--N export calibration and 0.35, 0.28, and -13.79% for validation, respectively.

Table 1. Optimum parameter values used in daily snowmelt runoff and NO_3^--N export calibration

Parameters	Definition	Optimal value
CNFROZ	A parameter to modify retention parameter for frozen conditions	0.000862
SMFMN	Minimum melt rate for snow during year (occurs on winter solstice) (mm/(℃.day))	4
SMFMX	Maximum melt rate for snow during year (occurs on summer solstice) (mm/(℃.day))	7
SMTMP	Snowmelt base temperature (℃)	0.5
SNO50COV	Fraction of SNOCOVMX that corresponds to 50% snow cover	0.12
SNOCOVMX	Minimum snow water content that corresponds to 100% snow cover (mm)	190
TIMP	Snowpack temperature gag factor	0.23
ALPHA_BF	Baseflow factor (day)	0.2
GW_DELAY	Delay time for aquifer recharge (days)	15
ESCO	Soil evaporation compensation factor	1
OV_N	Manning's value for overland flow	0.14
SURLAG	Surface runoff lag time (day)	0.1
CN2	SCS runoff curve number for moisture condition II	Maize field 56/ Forest 40
CH_K(1)	Effective hydraulic conductivity (mm/h)	2
CH_N(1)	Manning's value for the tributary channels	0.04
SDNCO	Denitrification threshold water content	0.92
SOL_NO3	Initial nitrate concentration in a soil layer (mg/kg)	15/10/5/3
NPERCO	Nitrogen percolation coefficient	0.7
ANION_EXCL	Fraction of porosity from which anions are excluded	0.2
CDN	Denitrification exponential coefficient	2.9

https://doi.org/10.5194/egusphere-2024-3984
Preprint. Discussion started: 28 January 2025

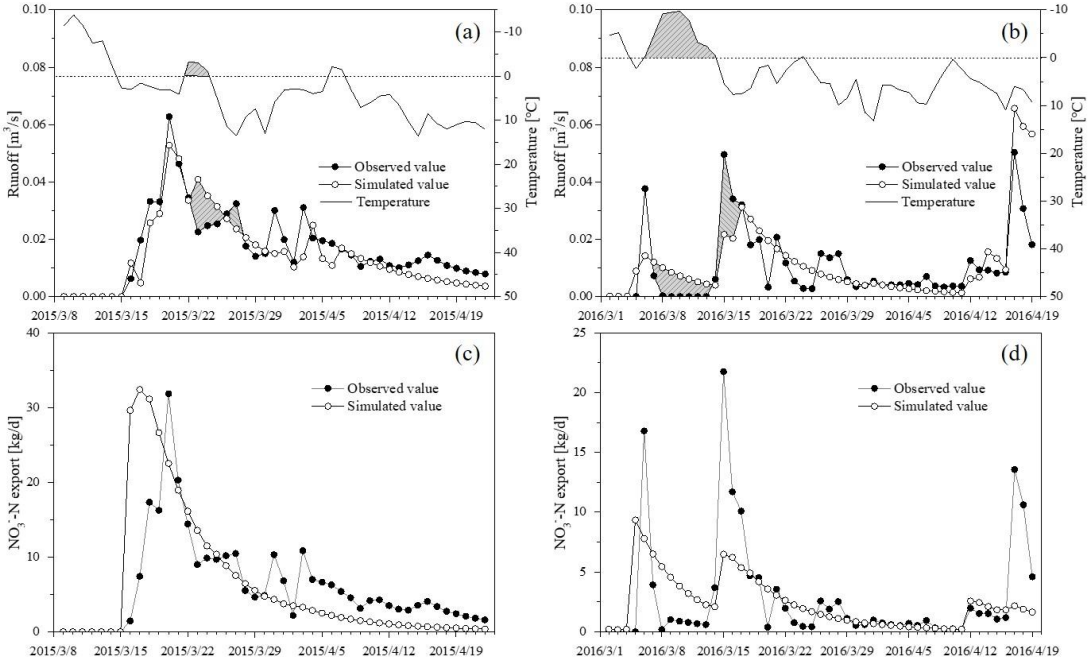

Fig. 4. Calibration and validation result of daily snowmelt runoff and NO_3^- -N export. Shadow areas denote the differences induced by temperature varation.

Table 2. Performance evaluation of SWAT model

Model evaluation statistics	Calibration （2014–2015）		Validation（2015–2016）	
	Runoff	NO_3^--N Export	Runoff	NO_3^--N Export
E_{NS}	0.75	-0.19 (0.66)[a]	0.54	0.35 (0.48)[a]
R^2	0.78	0.44 (0.46)[a]	0.51	0.28 (0.41)[a]
R_e	-12.76%	2.7%	15.65%	-13.79%

[a] *NSE* and R^2 values when simulated values during the initial snowmelt period were put off a day

3.2 Variation in climatic factors and the export of water and nitrogen

The variation and MK test values of modeling runoff, runoff coefficient, NO_3^--N export, starting Julian day, number of days of different freezing-thawing periods, corresponding accumulated precipitation, and average temperature from 1951–2014 were calculated (Fig. 5). The average runoff, runoff coefficient and NO_3^--N export in this watershed during the snowmelt period were 27758.5 m^3, 0.055, and 281.0 kg, respectively (Fig. 5a). The UF value of runoff was mostly between 0–1.96 from 1985–2014, which indicates that the trend of runoff increased since 1985, but was not obvious (Fig. 5f). The variation trend of the runoff coefficient was similar to that of runoff. The UF value of NO_3^--N export was mostly below 0 and even

https://doi.org/10.5194/egusphere-2024-3984
Preprint. Discussion started: 28 January 2025

lower than -1.96, thereby indicating that NO_3^--N export exhibited a decreasing trend during this period. Similarly, the average temperature of the three periods showed an increasing trend, and the increasing trend of the unstable and stable freezing periods reached a significant level (α = 0.05) around 1990 (Fig. 5g). Affected by the temperature rise trend, the stating days of stable freezing and snowmelt period (SD-SFP, SD-SMP) was advanced, and the advancement of the SD-SMP reached a significant level (α = 0.05) since 1996 (Fig. 5c and 5g). As a result, the number of days for the snowmelt period (ND-SMP) has significantly increased since 2000, and the number of days for the unstable and stable freezing periods (ND-USFP and ND-SFP) exhibit a decreasing trend (Fig. 5d and 5h). Accumulated precipitation has shown an increasing trend during the unstable, stable freezing, and snowmelt periods since 2009, 2009, and 1980, respectively.

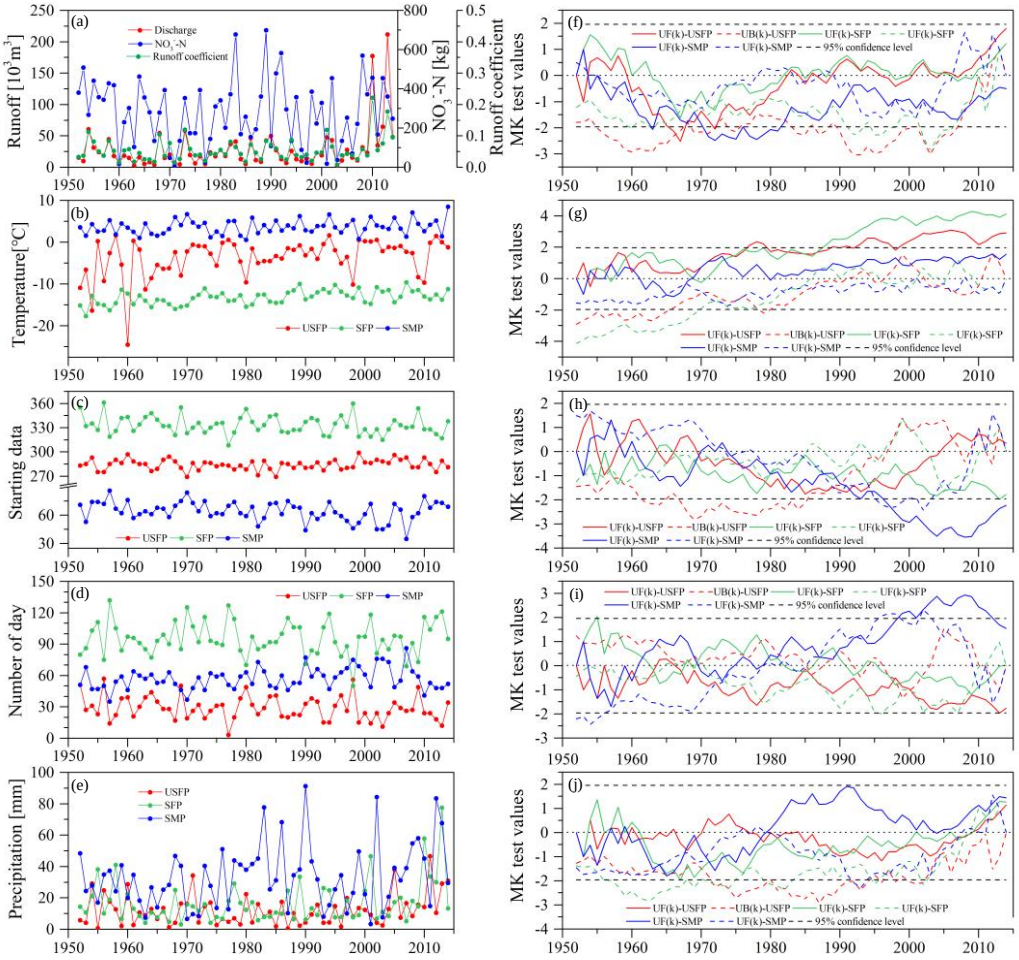

https://doi.org/10.5194/egusphere-2024-3984
Preprint. Discussion started: 28 January 2025

Fig. 5. Variation and MK test values of climatic factors during unstable freezing-thawing period (USFP), stable freezing-period (SFP), snowmelt period (SM) and the export of water and nitrogen during snowmelt period from 1951–2014.

3.3 Relationships between climate factors and the export of water and nitrogen

The relationships between the climatic factors are shown in Fig. 6. SD-SMP was significantly positively correlated with ND-SFP and average temperature during the snowmelt period (T-SMP) ($p < 0.001$), and negatively correlated with the average temperature of the stable freezing period (T-SFP) ($p < 0.001$). The ND-SFP was significantly positively correlated with precipitation during the stable freezing period (P-SFP) and T-SMP ($p < 0.001$), and negatively correlated with the negative cumulative temperature of the stable freezing period ($p < 0.001$). These relationships are graphically represented in Fig. 7.

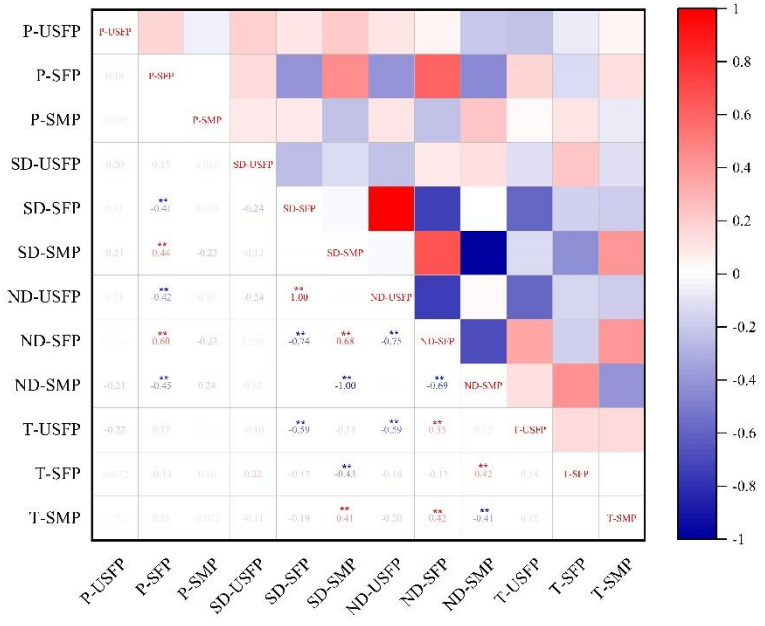

https://doi.org/10.5194/egusphere-2024-3984
Preprint. Discussion started: 28 January 2025

Fig. 6. Co-relationships between precipitation (P), starting day (SD), number of day (ND), and average temperature (T) of the unstable freezing period (USFP), stable freezing period (SFP), and snowmelt period (SMP).

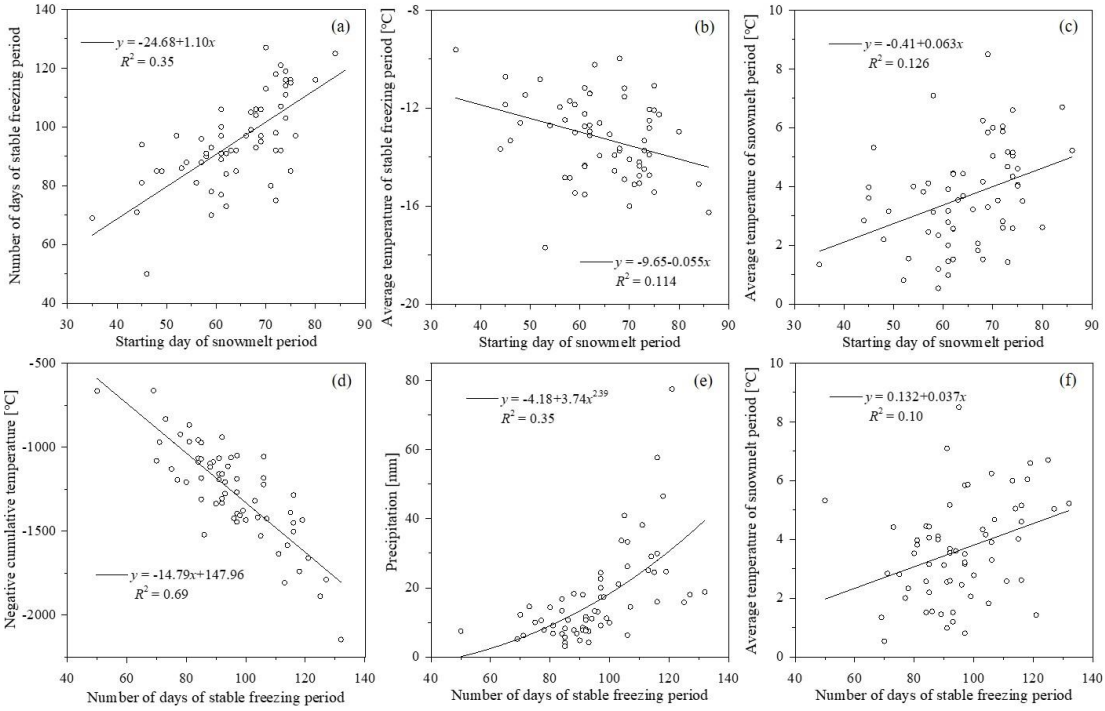

Fig. 7. Relationship between climatic factors.

Due to the strong collinearity between climate factors, the coefficients of principal component regression between climate factors and runoff, runoff coefficient, and NO_3^--N export were calculated to evaluate the magnitude of their impact (Fig. 8). All of the fits reached significance levels ($p < 0.001$ for runoff and runoff coefficient, and $p < 0.05$, for NO_3^--N export); therefore, the magnitude of the regression coefficients can be used to characterize the impact of climate factors on runoff, runoff coefficient, and NO_3^--N export. The P-SFP, precipitation ratio of the stable freezing period (P_{SFP}/P_{FT}) (PR-SFP), SD-SMP, and ND-SFP had greater positive effects on runoff and runoff coefficients, whereas ND-USFP and SD-SFP had greater negative effects on them (Fig. 8). The precipitation and precipitation ratio of snowmelt periods (P-SMP and PR-SMP) had greater positive effects on NO_3^--N export, while the precipitation and precipitation ratio of the unstable freezing period (P-USFP and PR-USFP) had greater negative effects on the same. The ND-SFP and PR-SMP are the most important factors affecting the runoff/runoff coefficient and NO_3^--N export, respectively.

https://doi.org/10.5194/egusphere-2024-3984
Preprint. Discussion started: 28 January 2025

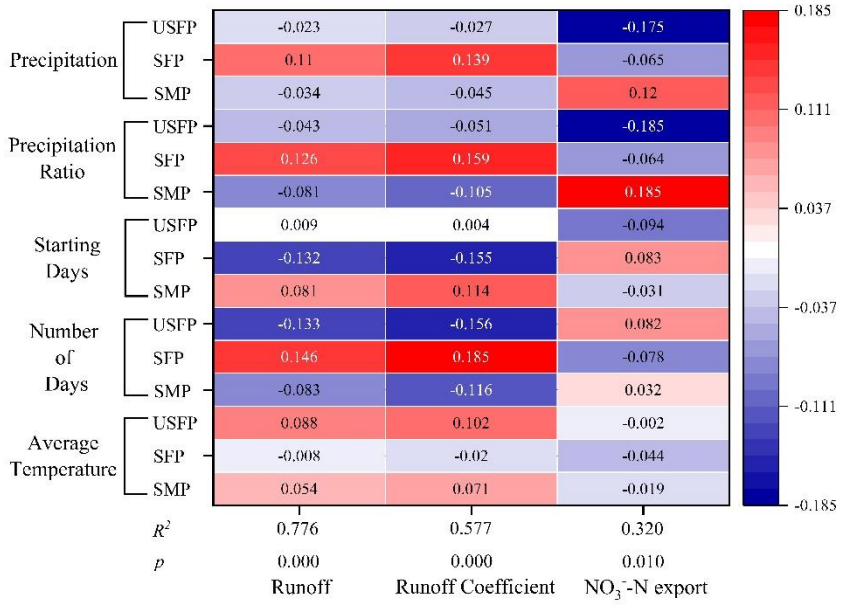

Fig. 8. Coefficients of principal component regression between runoff, runoff coefficient, NO_3^--N export, and climate factors [precipitation (P), precipitation ratio (PR), starting days (SD), number of days (ND), and average temperature (T)] in the unstable freezing period (USFP), stable freezing period (SFP), and snowmelt period (SMP).

The relationship between runoff, runoff coefficient, and NO_3^--N export with precipitation during different freeze-thaw periods is shown in Fig. 9. The runoff and runoff coefficients during the snowmelt period increased exponentially and linearly with increasing precipitation during the freezing-thawing period and stable freezing periods (Fig. 9a, 9b, 9d, and 9e), respectively. NO_3^--N export increased linearly with increasing precipitation during the freeze–thaw and snowmelt periods (Fig. 9c and 9f). Additionally, the fit coefficients of runoff, runoff coefficient, and NO_3^--N export with P-SFP and P-SMP were higher than those with precipitation during the freezing-thawing period.

https://doi.org/10.5194/egusphere-2024-3984
Preprint. Discussion started: 28 January 2025

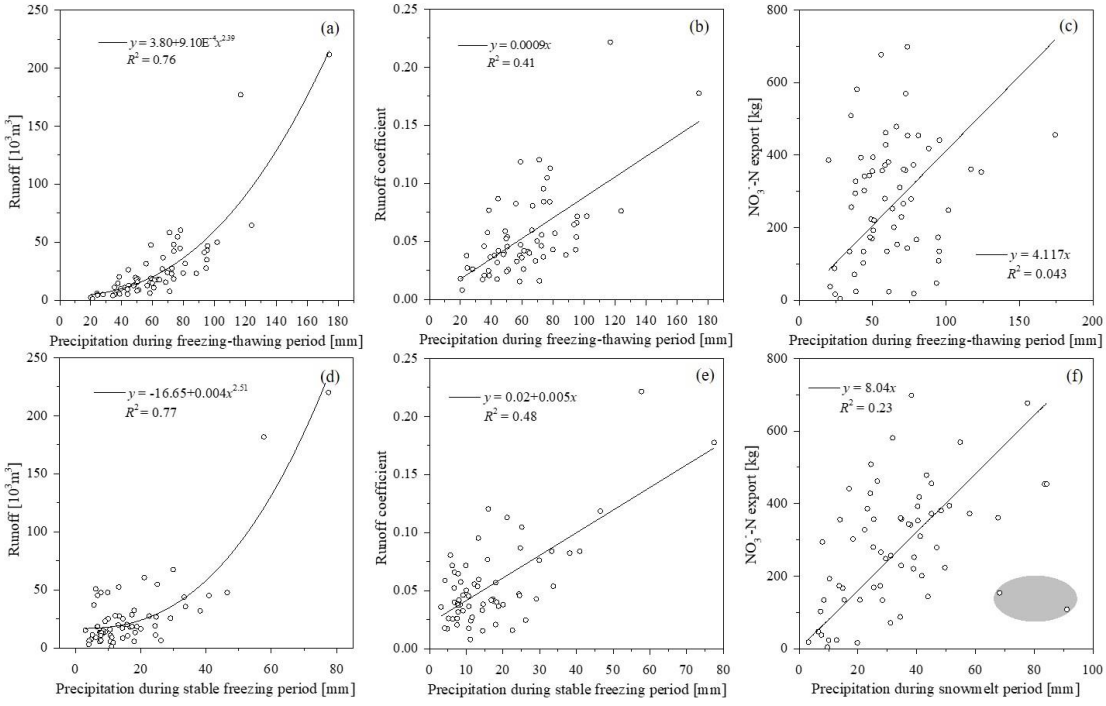

Fig. 9. Relationship of runoff, runoff coefficient, and nitrogen export with climatic factors.

4. Discussion

4.1 Applicability of SWAT model to simulate daily water and NO_3^--N export

SWAT model performs well in simulating the daily snowmelt runoff, and *NSE* and R^2 values are 0.75 and 0.78 for calibration, and 0.54 and 0.51 for validation, respectively (Fig. 4 and Table 2). The difference between simulated and observed values was mostly induced by overestimation of snowmelt runoff during some early snow-melting days when temperature dropped to <0 °C, and underestimation of the same during the flowing warmer days during both the calibration period (2014–2015) and validation period (2015–2016). This is because the runoff is mostly from surface flow, and interflow above frozen soil at the beginning of snowmelt (Zhao et al., 2017; Zhao et al., 2021). This surface water and near-surface soil water would be refrozen as ice when an in-between temperature drop event (<0 °C) occurred. Subsequently, the formation of ice would block the flow paths, which reduced or even restrained the generation of snowmelt runoff (Bengtsson, 1982; Zhao et al., 2022). The refrozen of snowmelt water was not considered in the SWAT model; therefore, these processes were not captured. However, these processes only changed the distribution of runoff over time but had little influence on the total amount of runoff. The R_e values were -12.76% and 15.65% for daily snowmelt runoff calibration and validation, respectively. This indicates that the SWAT model shows good performance in modeling the amount of snowmelt water.

https://doi.org/10.5194/egusphere-2024-3984
Preprint. Discussion started: 28 January 2025

NSE, and R^2 values of daily NO_3^--N export simulation are -0.19 and 0.44 for calibration, and 0.35 and 0.28 for validation, respectively, which are lower than those of daily snowmelt runoff simulation (Table 2). The lower *NSE* and R^2 values were mainly attributed to two reasons. As discussed above, the SWAT model does not consider the refrozen snowmelt water, which results in over- and underestimated NO_3^--N export during temperature drop and rise days during the initial snowmelt period (Bengtsson, 1982; Nie et al., 2017). The beginning of water and NO_3^--N export was earlier and higher in modeling value (Fig. 3) because the SWAT model did not involve the hysteresis effect of snow cover in the river channel on snowmelt runoff (Ouyang et al., 2013; Nie et al., 2017). If the simulated values of daily NO_3^--N export during the initial snowmelt period were put off a day and then compared with the observed values, the *NSE* and R^2 could reach 0.46 and 0.66 for calibration, and 0.41 and 0.48 for validation (Table 3), respectively. Only the total amount of NO_3^--N export was considered in the latter parts, and the R_e values were 2.7% and -13.79% for daily NO_3^--N export calibration and validation, respectively. Hence, the SWAT model is considered suitable for simulating daily NO_3^--N export during the snowmelt period.

4.2 Combination of different climate factors that facilitate snowmelt runoff

The snowmelt runoff and the runoff coefficient during the snowmelt period were significantly positively correlated with ND-SFP, PR-SFP, P-SFP, and SD-SMP, and negatively correlated with ND-USFP, ND-SMP, and SD-SFP (Figs. 8 and 9). This could have occurred because the earlier SD-SFP and later SD-SMP were always accompanied by colder and longer stable freezing periods (Figs. 6 and 7b), which led to lower negative cumulative temperature (Fig. 7d) and higher accumulated precipitation during the stable freezing period (Fig. 7e). A lower negative cumulative temperature induces more soil water to move upward during the soil freezing process (Butler et al., 1996; Wu et al., 2019). This is associated with higher accumulated precipitation to increase the amount of surface water available for runoff generation during the snowmelt period. Low-temperature cold also induces severe freezing soil, prevents the infiltration of snowmelt water, and prolongs surface and interflow processes (Zhao et al., 2017). Furthermore, the number of days of stable freezing was significantly positively correlated with the average temperature of the snowmelt period (Fig. 7f), thereby indicating that a longer stable freezing period is always accompanied by warmer temperatures during the snowmelt period. Therefore, the accumulated snow melts in a shorter time period and induces a more significant snowmelt runoff (Zhao et al., 2021). These combined effects increased the runoff coefficient and finally increased the snowmelt runoff. Therefore, the relationship between the runoff coefficient and precipitation during the stable freezing period was even better than that with precipitation during the freezing-thawing period (Fig. 9).

To verify this conjecture, the variation in climate factors during the freezing-thawing period and daily snowmelt runoff during the snowmelt period for years with the highest runoff coefficient are shown in Fig. 9 of which four years had the highest runoff (Fig. 9a–9d). The average ND-SFP and SD-SMP of these 8 years was 112.62 and 73.25 days, which were 17.20 days longer and 8.95 days later, respectively, than the average value of the same in 1951–2014. In addition, the average PR-SFP of these eight years was 41.34%, which was 1.48 times of the average value for 1951–2014. On this basis,

https://doi.org/10.5194/egusphere-2024-3984
Preprint. Discussion started: 28 January 2025

runoff and runoff would be quite high if rain-on-snowmelt events occurred during the snowmelt period (Fig. 9a–9d). Therefore, based on the analysis of runoff and climate factor data from long series and typical years, it can be concluded that the years with a longer stable freezing period, later snowmelt period starting day, and higher rainfall during snowmelt are more likely to generate high snowmelt runoff.

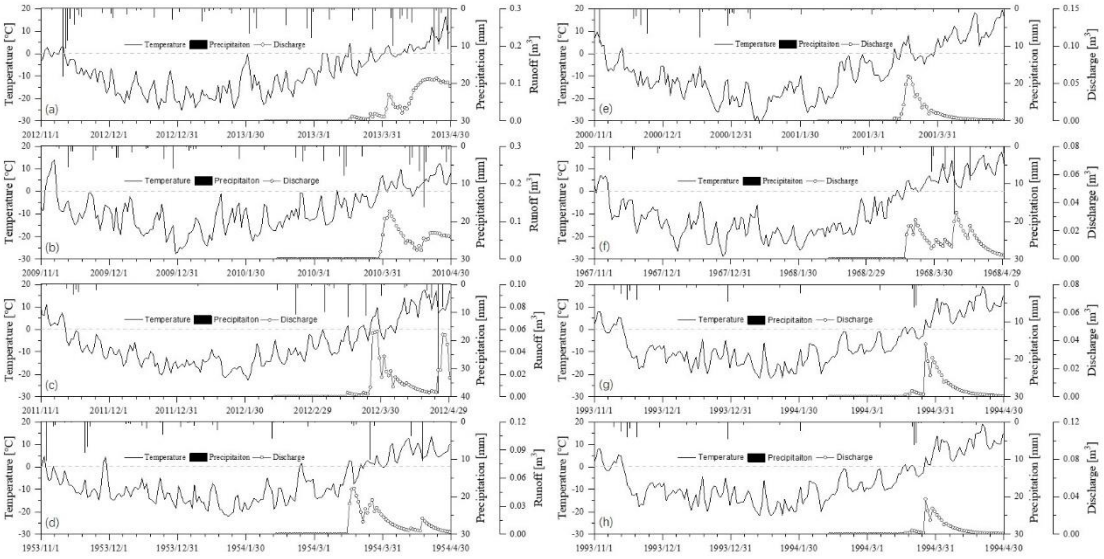

Fig. 10. Variation of climate factors and daily snowmelt runoff during freezing-thawing period for years with highest runoff (Fig. 9a–9d) and runoff coefficient (Fig. 9a–9h).

4.3 Combination of different climatic factors that facilitate NO_3^--N export

The daily NO_3^--N export during the snowmelt period had a poor relationship with snowmelt runoff (Fig. A1) and precipitation during the entire freezing-thawing period (Fig. 9c). Meanwhile, they were significantly positively affected by P-SMP and PR-SMP (Figs. 8and 9f), which indicates that NO_3^--N may be mainly exported during runoff generated by rainfall during the snowmelt period.

Variations in climate factors and daily NO_3^--N export during the freeze-thaw period with the highest NO_3^--N export are shown in Fig.11. The average T-SMP, P-SMP, and PR-SMP of these years were 5.32 ℃, 50.63 mm and 64.70%, which were 1.46, 1.51 and 12.3 times the average value of 1951–2014, respectively. Furthermore, most of the precipitation during the snowmelt period in these years occurred after April 20, and the time between rainfall and snowmelt was long and the temperature during this time was high. This was because the temperature was lower during the freezing and early snowmelt periods, and the soil air permeability was restricted by frozen soil and snowmelt water (Larsbo et al., 2019), which would inhibit the activity of nitrifying bacteria, enhance the activity of denitrifying bacteria, and finally inhibit the formation of NO_3^--N (Zhao et al., 2019; Jiang et al., 2020). The limited NO_3^--N was mostly flushed into rivers by snowmelt during the early snowmelt period, and the watershed may have been short of NO_3^--N for a period of time immediately after snowmelt

https://doi.org/10.5194/egusphere-2024-3984
Preprint. Discussion started: 28 January 2025

events (Zhao et al., 2017). The nitrate-nitrogen concentration decreased exponentially with increasing runoff (Fig A2). Therefore, later rain events and higher temperatures between the snowmelt and rain events would create a soil environment with warmer temperatures and higher air permeability, which is favored by the formation of NO_3^--N (Zhao et al., 2019; Xu, 2022). Furthermore, fertilizer application between April 5th and 20th during the spring plowing event further increased the NO_3^--N content in the watershed. High and concentrated rainfall events during the late snowmelt period provided a driving force for the export of NO_3^--N. Therefore, later appeared (after April 20), higher and concentrated rainfall events, and higher temperatures between these rainfall events and snowmelt events favored the combination of NO_3^--N export.

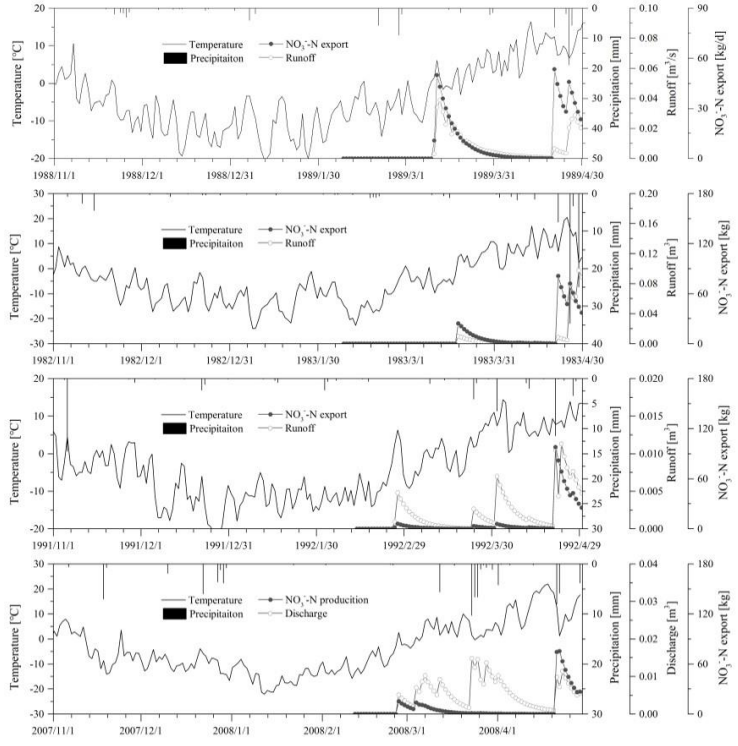

Fig. 11. Variation of climate factors, daily snowmelt runoff, and daily NO_3^--N export during the freezing-thawing period of years with highest NO_3^--N export.

4. Conclusion

This study evaluated the application of the SWAT model to simulate the daily water and NO_3^--N export during the snowmelt period, identified the controlling climate factors, and confirmed their suitable combination to facilitate snowmelt water and NO_3^--N export. We found that the SWAT model performed well for *Re* values in simulating the daily snowmelt runoff and NO_3^--N export, but poorly for *NSE* and R^2 values in simulating NO_3^--N export. ND-SFP and P-SFP controlled daily snowmelt runoff, while daily NO_3^--N export was mostly affected by P-SMP. The combinations of climatic factors favored by snowmelt runoff and NO_3^--N export were different. Years with longer ND-SFP and later SD-SMP were always accompanied

https://doi.org/10.5194/egusphere-2024-3984
Preprint. Discussion started: 28 January 2025

by higher P-SFP and lower negative cumulative temperature, which increased the amount of surface water available for runoff generation and the runoff coefficient. These combined effects increased the snowmelt runoff. Later appeared rainfall and higher temperature favored the formation of NO_3^--N during snowmelt period. High and concentrated rainfall events during the late snowmelt period provided a driving force for the export of these NO_3^--N. This research provides new insights into the effects of climate change on snowmelt runoff and accompanying NO_3^--N generation.

Data availability

All raw data can be provided by the corresponding authors upon request.

Author contributions

QZ, DC, and JWW planned the research; ZYP, DC, QY, CYG, and CGL performed the measurements; QZ, DC, and ZYP analyzed the data; QZ and DC wrote the manuscript draft; JWW, ZYP, QY, CYG and CGL reviewed and edited the manuscript.

Competing interests

The authors declare that they have no conflict of interest.

Acknowledgments:

This research was jointly supported by the China Three Gorges Corporation Research Project (NBWL202300014，NBWL202300013), the project of Key Laboratory of Changjiang Regulation and Protection of Ministry of Water Resources (CX2023K02), and the National Natural Science Foundation of China (No. 52109063).

References

Appels W. M., Coles A. E., Mcdonnell J. J.: Infiltration into frozen soil: from core-scale dynamics to hillslope-scale connectivity. Hydrol. Process 32 (1), 66-79, doi.org/10.1002/hyp.11399, 2018.

Arnold J. G., Moriasi D. N., Gassman P. W., Abbaspour K. C., White M. J., Srinivasan R., Santhi C, Harmel RD, van Griensven A., Van Liew M. W., Kannan N., Jha M. K.: SWAT: model use, calibration, and validation. T. Asabe. 55 (4), 1491-1508, doi.org/10.13031/2013.42256, 2012.

Aygun O., Kinnard C., Campeau S.: Impacts of climate change on the hydrology of northern midlatitude cold regions. Prog. Phys. Geog. 44 (3), 338-375, doi.org/10.1177/0309133319878123, 2020.

Bengtsson L.: The importance of refreezing on the diurnal snowmelt cycle with application to a northern Swedish catchment. Hydrol. Res. 13 (1), 1-12, doi.org/10.2166/nh.1982.0001, 1982.

https://doi.org/10.5194/egusphere-2024-3984
Preprint. Discussion started: 28 January 2025

Bhatta B., Shrestha S., Shrestha P. K., Talchabhadel R.: Evaluation and application of a swat model to assess the climate change impact on the hydrology of the Himalayan river basin. Catena 181, doi.org/10.1016/j.catena.2019.104082, 2019.

Bing H., He P., Zhang Y.: Cyclic freeze–thaw as a mechanism for water and salt migration in soil. Environ. Earth. Sci. 74, 675–681 (2015), doi.org/10.1007/s12665-015-4072-9, 2015.

Butler A. P., Burne S., Wheater H.S.: Observations of 'freezing-induced redistribution' in soil lysimeters. Hydrol. Process 10 (3), 471-474, doi.org/10.1002/(SICI)1099-1085(199603)10:3<471::AID-HYP317>3.0.CO;2-3, 1996.

Cao J., Liu C., Zhang W.: Response of rock-fissure seepage to snowmelt in mount Taihang slope-catchment, North China. Water Sci. Technol. 67 (1), 124-130, doi.org/10.2166/wst.2012.542, 2013.

Chen C., Yu Z., Xiang L., He J., Fu X.: Effects of rainfall intensity and amount on the transport of total nitrogen and phosphorus in a small agricultural watershed, In: Jiang CB, Yang ZJ (Eds.), Advances in Hydrology and Hydraulic Engineering, PTS 1 and 2, International Conference on Civil, Architectural and Hydraulic Engineering (ICCAHE 2012), PP. 268-271, doi.org/10.4028/www.scientific.net/AMM.212-213.268, 2012.

Clement J. C., Robson T. M., Guillemin R., Saccone P., Lochet J., Aubert S., Lavorel S.: The effects of snow-n deposition and snowmelt dynamics on soil-n cycling in marginal terraced grasslands in the french alps. Biogeochemistry 108 (1), 297-315, doi.org/10.1007/s10533-011-9601-3, 2012.

Corriveau J., Chambers P. A., Yates A. G., Culp J. M.: Snowmelt and its role in the hydrologic and nutrient budgets of prairie streams. Water Sci. Technol. 64 (8), 1590-1596, doi.org/10.2166/wst.2011.676, 2011.

Dibike Y.., Muhammad A., Shrestha R. R., Spence C., Bonsal B., de Rham L., Rowley J., Evenson G., Stadnyk T.: Application of dynamic contributing area for modelling the hydrologic response of the Assiniboine river basin to a changing climate. J. Great Lakes Res. 47 (3), 663-676, doi.org/10.1016/j.jglr.2020.10.010, 2021.

Dou T., Xiao C., Liu J., Wang Q., Shifeng P., Su J., Yuan X., Ding M., Zhang F., Xue K., Bieniek P., Eicken H.: Trends and spatial variation in rain-on-snow events over the arctic ocean during the early melt season. The Cryosphere, 15, 883–895, doi.org/10.5194/tc-15-883-2021, 2021.

Grusson Y., Sun X., Gascoin S., Sauvage S., Raghavan S., Anctil F., Sáchez-Pérez J.: Assessing the capability of the swat model to simulate snow, snow melt and streamflow dynamics over an alpine watershed. J. Hydrol. 531, 574-588, doi.org/10.1016/j.jhydrol.2015.10.070, 2015.

He S., Gong Y., Zheng Z., Luo Z., Tan B., Zhang Y.: Effects of rainfall intensities and slope gradients on nitrogen loss at the seedling stage of maize (zea mays l.) In the purple soil regions of China. Int. J. Agr. Biol. Eng. 15 (2), 142-148, doi.org/10.25165/j.ijabe.20221502.6015, 2022.

Heggli A., Hatchett B., Schwartz A., Bardsley T., Hand E.: Toward snowpack runoff decision support. iScience 25 (5), 104240. doi.org/10.1016/j.isci.2022.104240, 2022.

Ipcc (2018) global warming of 1.5°c.an ipcc special report on the impacts of global warming of 1.5°c above pre-industrial levels and related global greenhouse gas emission pathways, in the context of strengthening the global response to the threat

https://doi.org/10.5194/egusphere-2024-3984
Preprint. Discussion started: 28 January 2025

of climate change, sustainable development, and efforts to eradicate poverty. World Meteorological Organization, Geneva, Switzerland, P. 32p.

Irannezhad M., Ronkanen A. K., Kiani S., Chen D., Klove B.: Long-term variability and trends in annual snowfall/total precipitation ratio in Finland and the role of atmospheric circulation patterns. Cold Reg. Sci. Technol. 143 (nov.), 23-31, doi.org/10.1016/j.coldregions.2017.08.008, 2017.

Ireson A. M., Kamp G. V. D, Ferguson G., Nachshon U., Wheater H. S.: Hydrogeological processes in seasonally frozen northern latitudes: understanding, gaps and challenges. Hydrogeol. J. 21 (1), 53-66, doi.org/10.1007/s10040-012-0916-5, 2013.

Jiang N., Juan Y., Tian L., Chen X., Sun W., Chen L.: Soil water contents control the responses of dissolved nitrogen pools and bacterial communities to freeze-thaw in temperate soils. Biomed. Res. Int. 2020, 1-10, doi.org/10.1155/2020/6867081, 2020.

Klein G., Vitasse Y., Rixen C., Rixen C., Marty C., Rebetez M.: Shorter snow cover duration since 1970 in the Swiss Alps due to earlier snowmelt more than to later snow onset. Clim. Change 139, 637–649, doi.org/10.1007/s10584-016-1806-y, 2016.

Koch J. C., Ewing S. A., Striegl R., Mcknight D. M.: Rapid runoff via shallow throughflow and deeper preferential flow in a boreal catchment underlain by frozen silt (Alaska, USA). Hydrogeol. J. 21 (1), 93-106, doi.org/10.1007/s10040-012-0934-3, 2013.

Koch J. C., Kikuchi C. P., Wickland K. P., Schuster P.: Runoff sources and flow paths in a partially burned, upland boreal catchment underlain by permafrost. Water Resour. Res. 50 (10), 8141-8158, doi.org/10.1002/2014WR015586, 2015.

Larsbo M., Holten R., Stenrod M., Eklo O. M., Jarvis N.: A dual-permeability approach for modeling soil water flow and heat transport during freezing and thawing. Vadose Zone J 18 (1), doi.org/10.2136/vzj2019.01.0012, 2019.

Levesque E., Anctil F., van Griensven A., Beauchamp N.: Evaluation of streamflow simulation by swat model for two small watersheds under snowmelt and rainfall. Hydrolog. Sci. J. 53 (5), 961-976, doi.org/10.1623/hysj.53.5.961, 2008.

Li B., Chen Y., Xiong H.: Quantitatively evaluating the effects of climate factors on runoff change for Aksu river in Northwestern China. Theor. Appl. Climatol. 123 (1-2), 97-105, doi.org/10.1007/s00704-014-1341-6, 2016.

Li H., Liu G., Han C., Yang Y., Chen R.: Quantifying the trends and variations in the frost-free period and the number of frost days across china under climate change using era5-land reanalysis dataset. Remote Sens-Basel 14 (10), 2400, doi.org/10.3390/rs14102400, 2022.

Ligare S. T., Viers J. H., Null S. E., Rheinheimer D. E., Mount J. F.: Non-uniform changes to whitewater recreation in California's sierra nevada from regional climate warming. River Res. Appl. 28 (8), 1299-1311, doi.org/10.1002/rra.1522, 2012.

Lone S. A., Jeelani G., Deshpande R. D., Mukherjee A., Jasechko S., Lone A.: Meltwaters dominate groundwater recharge in cold arid desert of upper Indus river basin (uirb), western Himalayas. Sci. Total Environ. 786, doi.org/10.1016/j.scitotenv.2021.147514, 2021.

https://doi.org/10.5194/egusphere-2024-3984
Preprint. Discussion started: 28 January 2025

Mukundan R., Linh H., Gelda R. K., Yeo M., Owens E. M.: Climate change impact on nutrient loading in a water supply watershed. J. Hydrol. 586, doi.org/10.1016/j.jhydrol.2020.124868, 2020.

Nash J. E., Sutcliffe J. V.: River flow forecasting through conceptual models part i — a discussion of principles. J. Hydrol. 10 (3), 282-290, doi.org/10.1016/0022-1694(70)90255-6, 1970.

Nie W., Krautblatter M., Leith K., Thuro K., Festl J.: A modified tank model including snowmelt and infiltration time lags for deep-seated landslides in alpine environments (Aggenalm, Germany). Nat. Hazard Earth Sys. 17 (9), 1595-1610, doi.org/10.5194/nhess-17-1595-2017, 2017.

Ouyang W., Huang H., Hao F., Guo B.: Synergistic impacts of land-use change and soil property variation on non-point source nitrogen pollution in a freeze-thaw area. J. Hydrol. 495, 126-134, doi.org/10.1016/j.jhydrol.2013.04.037, 2013.

Pittman F., Mohammed A., Cey E.: Effects of antecedent moisture and macroporosity on infiltration and water flow in frozen soil, Hydrol. Process 34 (3), 795-809. doi.org/10.1002/hyp.13629, 2020.

Ploum S. W., Lyon S. W., Teuling A. J., Laudon H., van der Velde Y.: Soil frost effects on streamflow recessions in a sub-arctic catchment. Hydrol. Process 33 (9), 1304-1316, doi.org/10.1002/hyp.13401, 2019.

Qin Y., Abatzoglou J. T., Siebert S., Huning L. S., Aghakouchak A., Mankin J. S., Hong C., Tong D., Davis S. J., Mueller N. D.: Agricultural risks from changing snowmelt. Nat. Clim. Change 10 (5), 459, doi.org/10.1038/s41558-020-0746-8, 2020.

Räisänen J., Eklund J.: 21st century changes in snow climate in northern Europe: a high-resolution view from ensembles regional climate models. Clim. Dynam. 38 (11), 2575-2591, doi.org/10.1007/s00382-011-1076-3, 2011.

Rasouli K., Pomeroy J. W., Marks D. G.: Snowpack sensitivity to perturbed climate in a cool mid-latitude mountain catchment. Hydrol. Process 29 (18), 3925-3940, doi.org/10.1002/hyp.10587, 2015.

Rattan K. J., Corriveau J. C., Brua R. B., Culp J. M., Yates A. G., Chambers P. A.: Quantifying seasonal variation in total phosphorus and nitrogen from prairie streams in the red river basin, Manitoba Canada. Sci. Total Environ. 575, 649-659, doi.org/10.1016/j.scitotenv.2016.09.073, 2017.

Rheinheimer D. E., Viers J. H., Sieber J., Kiparsky M.., Mehta V. K, Ligare S. T.: Simulating high-elevation hydropower with regional climate warming in the west slope, Sierra Nevada. J Water Res Plan Man 140 (5), 714-723, doi.org/10.1061/(ASCE)WR.1943-5452.0000373, 2014.

Romshoo S. A., Marazi A.: Impact of climate change on snow precipitation and streamflow in the Upper Indus Basin ending twenty-first century. Clim. Change 170, 6, doi.org/10.1007/s10584-021-03297-5, 2022.

Shi Y., Niu F., Lin Z., Luo J.: Freezing/thawing index variations over the circum-arctic from 1901 to 2015 and the permafrost extent. Sci. Total Environ. 660, 1294-1305, doi.org/10.1016/j.scitotenv.2019.01.121, 2019.

Shrestha N. K., Wang J.: Water quality management of a cold climate region watershed in changing climate. J. Environ. Inform. 35 (1), 56-80, doi.org/10.3808/jei.201900407, 2020.

Shrestha R. R., Dibike Y. B., Prowse T. D.: Modeling climate change impacts on hydrology and nutrient loading in the upper Assiniboine catchment. J Am. Water Resour. As. 48 (1), 74-89, doi.org/10.1111/j.1752-1688.2011.00592.x, 2012.

https://doi.org/10.5194/egusphere-2024-3984
Preprint. Discussion started: 28 January 2025

Sterle K., Hatchett B. J., Singletary L., Pohll G.: Hydroclimate variability in snow-fed river systems: local water managers' perspectives on adapting to the new normal. B. Am. Meteorol. Soc. 100 (6), 1029-1048, doi.org/10.1175/BAMS-D-18-0031.1, 2019.

Uzun S., Tanir T., Coelho G. D. A., Souza De Lima A. D.., Cassalho F, Ferreira C. M.: Changes in snowmelt runoff timing in the contiguous United States, Hydrol. Process. 35 (11). doi.org/10.1002/hyp.14430, 2021.

Van Liew M. W. Arnold J. G., Garbrecht J. D.: Hydrologic simulation on agricultural watersheds: choosing between two models. Transactions of the Asia 46 (6), 1539-1551, doi.org/10.13031/2013.15643, 2003.

Vorkauf M., Marty C., Kahmen A., Hiltbrunner E.: Past and future snowmelt trends in the Swiss Alps: the role of temperature and snowpack. Climatic Change 165, 44, doi.org/10.1007/s10584-021-03027-x, 2021.

Wang Y., Bian J., Zhao Y., Tang J., Jia Z.: Assessment of future climate change impacts on nonpoint source pollution in snowmelt period for a cold area using SWAT. Sci. Rep.-U.k. 8 (1), doi.org/10.1038/s41598-018-20818-y, 2018.

Wright N., Quinton W. L., Hayashi M.: Hillslope runoff from an ice-cored peat plateau in a discontinuous permafrost basin, Northwest territories, Canada. Hydrol. Process 22 (15), 2816-2828, doi.org/10.1002/hyp.7005, 2010.

Wu. M., Huang J., Tan X., Wu J.: Water, salt and heat influences on carbon and nitrogen dynamics in seasonally frozen soils in Hetao irrigation district, Inner Mongolia, China. Pedosphere 29 (5), 632-641, doi.org/10.1016/S1002-0160(17)60463-6, 2019.

Xu X.: Effect of freeze-thaw disturbance on soil c and n dynamics and ghg fluxes of East Asia forests: review and future perspectives. Soil science and plant nutrition (Tokyo) 68 (1), 15-26, doi.org/10.1080/00380768.2021.2003164

Yang Y., Chen R., Liu G., Liu Z., Wang X.: Trends and variability in snowmelt in China under climate change. Hydrol. Earth Syst. Sc. 26 (2), 305-329, doi.org/10.5194/hess-26-305-2022, 2022.

Zaremehrjardy M., Victor J., Park S., Smerdon B., Alessi D. S., Faramarzi M.: Assessment of snowmelt and groundwater-surface water dynamics in mountains, foothills, and plains regions in northern latitudes. J. Hydrol. 606, doi.org/10.1016/j.jhydrol.2022.127449, 2022.

Zhang Z., Wang W., Gong C., Wang Z., Duan L., Yeh T. J., Yu P.: Evaporation from seasonally frozen bare and vegetated ground at various groundwater table depths in the ordos basin, northwest China. Hydrol. Process 33 (9), 1338-1348, doi.org/10.1002/hyp.13404, 2019.

Zhao Q., Chang D., Wang K., Huang J.: Patterns of nitrogen export from a seasonal freezing agricultural watershed during the thawing period. Sci. Total Environ. 599, 442-450, doi.org/10.1016/j.scitotenv.2017.04.174, 2017.

Zhao Q., Guo C., Zeng Q., Zhao H., Liu Y., Zhang J., Huang J., Wu J.: Nitrogen migration paths and source areas at different snowmelt periods in a seasonal freezing agricultural watershed. J. Hydrol.-Reg. Stud. 41, 101083, doi.org/doi.org/10.1016/j.ejrh.2022.101083, 2022.

Zhao Q., Tan X., Zeng Q., Zhao H., Wu J., Huang J.: Combined effects of temperature and precipitation on the spring runoff generation process in a seasonal freezing agricultural watershed. Environ. Earth Sci. 80 (15), doi.org/10.1007/s12665-021-09777-2, 2021.

https://doi.org/10.5194/egusphere-2024-3984
Preprint. Discussion started: 28 January 2025

Zhao Q., Wu C., Wang K., Chang D., Huang J.: In situ experiment on change law of soil mineral nitrogen availability in seasonal freezing agricultural areas. Trans. Chin. Soc. Agric. Eng. 35 (17), 140-146. (In Chinese)

https://doi.org/10.5194/egusphere-2024-3984
Preprint. Discussion started: 28 January 2025

Appendix

Table A1. Description and range of parameters used in the calibration of hydrology

Order	Parameters	Definition	Range	Default	S_{AF}	
					Parameters +20%	Parameters -20%
1	CN2	SCS runoff curve number for moisture condition II	30–95	-	3.70	-1.43
2	CNFROZ	A parameter to modify retention parameter for frozen conditions	-	0.000862	-0.51	0.76
3	SNOCOVMX	Minimum snow water content that corresponds to 100% snow cover (mm)	-	1	-0.33	0.52
4	SNO50COV	Fraction of SNOCOVMX that corresponds to 50% snow cover	0.01–0.99	0.5	-0.36	0.51
5	SMFMX	Maximum melt rate for snow during year (occurs on summer solstice) (mm/(℃.day))	0–10	4.5	0.47	-0.40
6	TIMP	Snowpack temperature gag factor	0.01–1.0	1	0.44	-0.33
7	SMFMN	Minimum melt rate for snow during year (occurs on winter solstice) (mm/(℃.day))	0–10	4.5	0.30	-0.25
8	OV_N	Manning's value for overland flow	0–30	0.14	0.16	0.16
9	SURLAG	Surface runoff lag time (day)	-	2	0.07	0.16
10	SMTMP	Snowmelt base temperature (℃)	-5–5	0.5	-0.08	0.13
11	ESCO	Soil evaporation compensation factor	0–1	0.95	-	-0.08
12	GW_DELAY	Groundwater delay time (day)	-	31	-0.07	0.07
13	CH_K(1)	Effective hydraulic conductivity (mm/h)	-	-	0.03	0.02
14	ALPHA_BF	Baseflow factor (day)	0.1–1.0	0.048	0.02	-0.03
15	CH_N(1)	Manning's value for the tributary channels	0–30	0.014	0.02	-

https://doi.org/10.5194/egusphere-2024-3984
Preprint. Discussion started: 28 January 2025

Table A2. Description and range of parameters used in the calibration of nitrogen export

Order	Parameters	Definition	Range	Default	S_{AF}	
					Parameters +20%	Parameters +20%
1	CN2	SCS runoff curve number for moisture condition II	-	-	5.86	-1.10
2	SDNCO	Denitrification threshold water content	-	1.1	0.63	-4.58
3	CNFROZ	A parameter to modify retention parameter for frozen conditions	-	0.000862	-0.61	1.02
4	SOL_NO3	Initial nitrate concentration in a soil layer (mg/kg)	-	-	0.93	0.93
5	NPERCO	Nitrogen percolation coefficient	0.01–1.0	0.2	0.77	-0.81
6	TIMP	Snowpack temperature gag factor	0.01–1.0	1	0.69	-0.74
7	SMFMX	Maximum melt rate for snow during year (occurs on summer solstice) (mm/(℃.day))	0–10	4.5	0.44	-0.46
8	SMFMN	Minimum melt rate for snow during year (occurs on winter solstice) (mm/(℃.day))	0–10	4.5	0.33	-0.35
9	SNOCOVMX	Minimum snow water content that corresponds to 100% snow cover (mm)	-	1	-0.30	0.33
10	SNO50COV	Fraction of SNOCOVMX that corresponds to 50% snow cover	0.01–0.99	0.5	-0.25	0.25
11	SMTMP	Snowmelt base temperature (℃)	-5–5	0.5	-0.18	0.14
12	ESCO	Soil evaporation compensation coefficient	0–1	0.95		0.07
13	ANION_EXCL	Fraction of porosity from which anions are excluded	0–1	0.5	0.06	0.00
14	CDN	Denitrification exponential coefficient	1.4	1.4	-0.01	0.04
15	GW_DELAY	Delay time for aquifer recharge (days)	-	31	-0.03	-0.02

https://doi.org/10.5194/egusphere-2024-3984
Preprint. Discussion started: 28 January 2025

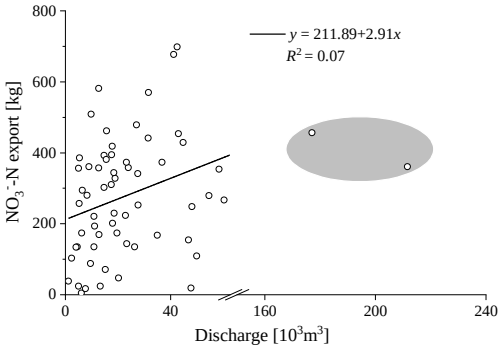

Fig. A1. Relationship of snowmelt runoff and NO_3^--N export.